ELSEVIER

TRM in low magnetic fields: a minimum field that can be recorded by large multidomain grains

Gunther Kletetschka [a,b,c,*], Michael D. Fuller [d], Tomas Kohout [b,e,f], Peter J Wasilewski [c], Emilio Herrero-Bervera [d], Norman F. Ness [g], M.H. Acuna [c]

[a] *Department of Physics, Catholic University of America, Washington D.C., USA*
[b] *Institute of Geology, Academy of Sciences, Prague, Czech Republic*
[c] *NASA Goddard Space Flight Center, Greenbelt, Maryland, USA*
[d] *Hawaii Institute of Geophysics and Planetology, University of Hawaii at Manoa, Honolulu, Hawaii, USA*
[e] *Department of Applied Geophysics, Charles University in Prague, Prague, Czech Republic*
[f] *Division of Geophysics, University of Helsinki, Finland*
[g] *Bartol Research Institute, University of Delaware, Newark, Delaware, USA*

Abstract

Thermally acquired remanent magnetization is important for the estimation of the past magnetic field present at the time of cooling. Rocks that cool slowly commonly contain magnetic grains of millimeter scale. This study investigated 1-mm-sized magnetic minerals of iron, iron–nickel, magnetite, and hematite and concluded that the thermoremanent magnetization (TRM) acquired by these grains did not accurately record the ambient magnetic fields less than 1 μT. Instead, the TRM of these grains fluctuated around a constant value. Consequently, the magnetic grain ability to record the ambient field accurately is reduced. Above the critical field, TRM acquisition is governed by an empirical law and is proportional to saturation magnetization (M_s). The efficiency of TRM is inversely proportional to the mineral's saturation magnetization M_s and is related to the number of domains in the magnetic grains. The absolute field for which we have an onset of TRM sensitivity is inversely proportional to the size of the magnetic grain. These results have implications for previous reports of random directions in meteorites during alternating field demagnetization, or thermal demagnetization of TRM. Extraterrestrial magnetic fields in our solar system are weaker than the geomagnetic field by several orders of magnitude. Extraterrestrial rocks commonly contain large iron-based magnetic minerals as a common part of their composition, and therefore ignoring this behavior of multidomain grains can result in erroneous paleofield estimates.
© 2006 Elsevier B.V. All rights reserved.

Keywords: TRM; Paleointensity; Meteorites; Multidomain magnetic minerals; Empirical law; Mars; Magnetism

1. Introduction

This work builds on the discovery of a new empirical scaling law relating the acquisition of thermal remanent magnetization, TRM, and saturation magnetization, M_s (Kletetschka et al., 2004). The law holds over the range of domain states from SD (single domain) to MD (multi domain) and strongly suggests that the demagnetization

* Corresponding author. Tel.: +1 301 286 3804.
  E-mail address: Gunther.Kletetschka@gsfc.nasa.gov
(G. Kletetschka).

energy must play an important role in TRM acquisition in all these grain sizes. Since the demagnetizing energy is proportional to $(M_s)^2$, it must compete at the blocking temperature with the energy of the external magnetic field. The importance of the demagnetizing energy was confirmed by experiments with samples with different demagnetizing factors. The empirical law suggests a generalized approach to models of TRM recognizing the importance of the demagnetizing energy with possible ramifications for paleointensity determinations.

Kletetschka et al. (2004) found a simple relationship between the efficiency of TRM (i.e., REM, the TRM to SIRM ratio) and the saturation magnetization of the material. The efficiency for equidimensional particles plots linearly with the magnetic field, B, along grain-size independent regions determined by the saturation magnetization of the material. For magnetite (grain size ranges from SD, through PSD (pseudo single domain) to MD) the efficiency is the same. The law further shows that the TRM intensity is particularly strong for minerals with low values of saturation magnetization might help to explain strong magnetization of titanohematite without need of "lamellar magnetism" (Robinson et al., 2002) following regular TRM acquisition principles (Kletetschka, 2000; Kletetschka et al., 2002).

Just below the Curie temperature the two dominant energies, independently of grain size, are the magnetostatic energy in the external field and magnetostatic energy in the demagnetizing field. The balance between the external field energy and demagnetizing energy at high temperature was a building block in models of multidomain TRM proposed by (Néel, 1949, 1955; Stacey, 1958). Indeed, it was shown in a review article by (Day, 1977) that the various multidomain models (Dunlop and Waddington, 1975; Everitt, 1962; Néel, 1955; Schmidt, 1973; Stacey, 1958), all followed this same approach with minor variations. Schmidt's model is perhaps the easiest to follow and emphasizes that at high temperature the critical energy balance is between the magnetostatic energy in the external and internal demagnetizing fields. Thus, the field, which ultimately controls the magnetization, is the effective field rather than the external field alone. The effective field is obtained in the usual way by subtracting the demagnetizing field from the external field. The demagnetizing factor is more complicated in multidomain grains than in homogenously magnetized particles (Merrill, 1977). However, given the recognition of the importance of the demagnetizing field, it is not too surprising that multidomain material follows the linear trends found by (Kletetschka et al., 2004). What is surprising is that such different grain sizes all show such similar behavior whether they are single domain, pseudo-single domain, or multidomain. This may all be pointing towards a more general approach to TRM that, at least at high temperature, depends upon the balance between magnetostatic energy in the external field and demagnetizing fields.

The single domain TRM model (Néel, 1949, 1955) is based upon thermal activation, and despite criticism (Brown, 1959) on the nature of the physics involved in determining the frequency factor, the approach has been extremely successful and has served as the foundation of magnetic theory in rock magnetism. The equilibrium magnetization (M) at temperature above the blocking temperature is given by Boltzmann statistics involving the hyperbolic tangent dependence on the ratio of the energy determining the alignment of the magnetization with H over the thermal kT_B energy.

$$M = M_s \tanh(\mu_0 V M_s H / k T_B) \tag{1}$$

where V is the volume of the particle, H the applied field, M_s the saturation magnetization, T_B the blocking temperature, and k Boltzmann's constant. However, given the recent results (Kletetschka et al., 2004), the demagnetizing energy must play an important role. This can be included in standard Néel theory by recognizing the importance of the demagnetizing energy in determining relaxation times, which follows the approach of Butler and Banerjee (1975) as well as Dunlop and Kletetschka (2001). In the Néel theory of MD grains, blocking occurs at T_B when barriers to wall motion increase according to coercivity $H_c(T)$ so that the domain walls pin against the demagnetizing field $H_d = -NM$ (N is the demagnetizing factor). TRM can be expressed as Dunlop and Kletetschka (2001):

$$M_{tr} = (1 - N\chi_0)n(n-1)^{1/n-1}H_{c0}^{1/n}N^{-1}H_0^{1-1/n} \tag{2}$$

and we obtain the theoretical value of M_{tr} just from the knowledge of the susceptibility χ_0, room temperature coercivity force H_{c0}, index n, applied field H_0 and demagnetization factor N. This theoretical curve is shown for hematite in Fig. 1A where $n = 3$, $H_{c0} = 4$ mT, and $N = 0.31$ (SI) see also Dunlop and Kletetschka (2001).

While the importance of demagnetizing energy is recognized, as for example in the excellent discussion by Dunlop and Ozdemir on pages 84–102 (Dunlop and Özdemir, 1997), it appears that the full significance of the demagnetizing energy and shape anisotropy has not been generally appreciated. If one calculates the balance between the magnetostatic energy in an applied weak field ($\sim$0.1 mT) and the demagnetizing energy, one finds that the magnetostatic energy in the external field only dominates for a few tenths of a degree below the
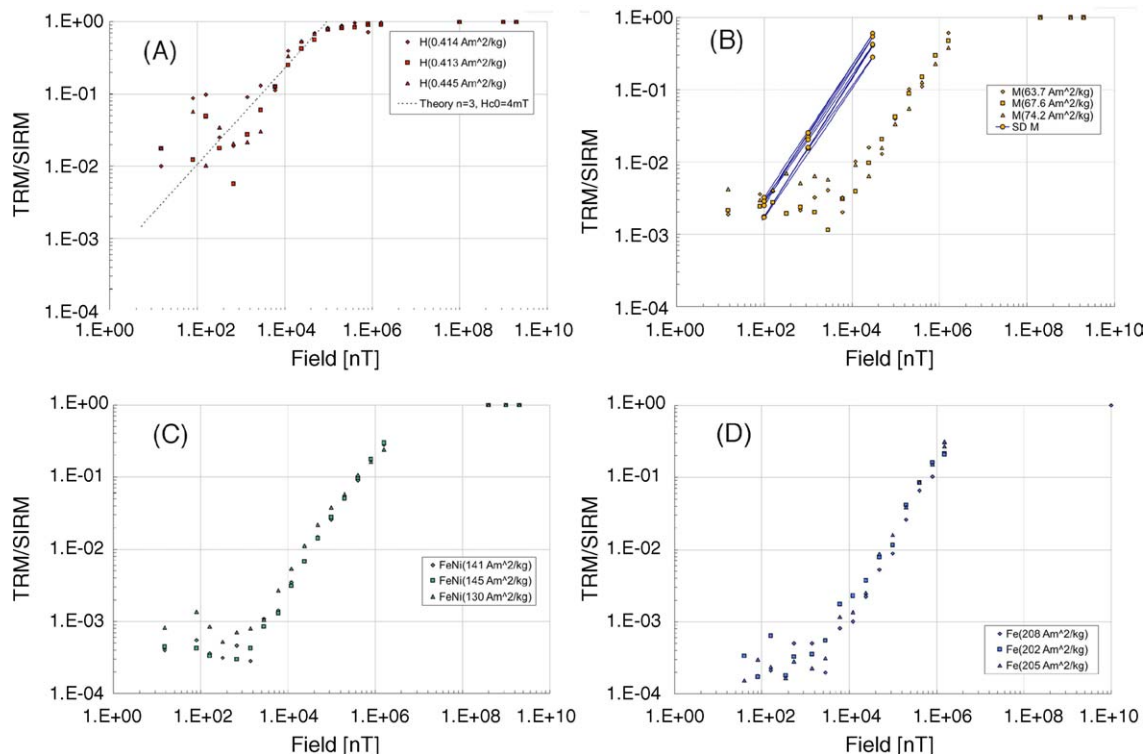
Fig. 1. Thermal remanent magnetizations (TRM) of multidomain minerals are normalized by saturation isothermal remanent magnetization (SIRM). Note that numbers shown in the legend are saturation magnetizations of individual samples. Horizontal axis represents inducing artificial homogeneous external magnetic field. (A) Magnetic acquisition of hematite; straight line is a theoretical prediction according to Dunlop and Kletetschka (2001) for $n = 3$, $H_{c0} = 4\,mT$, $N = 0.31$ (SI). (B) Magnetite; circles connected with lines are SD magnetite needles within anorthosite matrix (see the text for further explanation). (C) Iron–nickel. (D) Iron.

Curie point, so that the TRM can be regarded as a departure from saturation magnetization towards equilibrium driven by the demagnetizing energy. This will be the case for PSD and MD particles. Moreover, both TRM and SIRMs are departures from saturation magnetization driven by demagnetizing energy. The difference is that TRM takes place over a range temperatures beginning close to the Curie point, but SIRM is acquired at the observation temperature. For SD particles the demagnetizing energy enters through the determination of the relaxation time, as suggested above.

2. Materials and methods

We performed a series of TRM acquisitions using five distinct magnetic materials: iron (Fe), iron–nickel (FeNi), magnetite (Fe_3O_4), hematite (α-Fe_2O_3), and sample of anorthosite from Archean Stillwater Complex (Bergh, 1970; Selkin et al., 2000; Xu et al., 1997) containing single domain (SD) magnetite as primary remanence carriers. The latter was kindly provided by Lisa Tauxe (Scripps Institution of Oceanography = SIO,

La Jolla, CA, USA). Former specimens were also used in Kletetschka et al. (2004). Magnetite and hematite samples were single crystals while iron and iron–nickel were polycrystalline. All specimens were about 1 mm in size except the host of SD magnetite, which consists of cumulate plagioclase matrix, and was of ~5 mm in diameter.

SD magnetite: Fragment was part of 1 in. core drilled in an unoriented anorthosite block sample (M428) from the Stillwater Complex (Selkin et al., 2000). This complex is an ultramafic to mafic intrusion in the Beartooth Mountains of southern Montana. Several lines of evidence suggest that single-domain magnetite is the dominant carrier of magnetic remanence. The specimens have high coercivity, with median destructive fields exceeding 80 mT pointing toward fine-grained, possibly single domain carrier (Selkin et al., 2000). TRM demagnetization (Selkin et al., 2000) indicates that more than 90% of remanence is unblocked between 550 and 575 °C pointing towards Ti-free magnetite. An observed inverse relationship between the AMS and remanence fabrics (Selkin et al., 2000) provides compelling evidence that the remanence carrier contains primarily single domains.
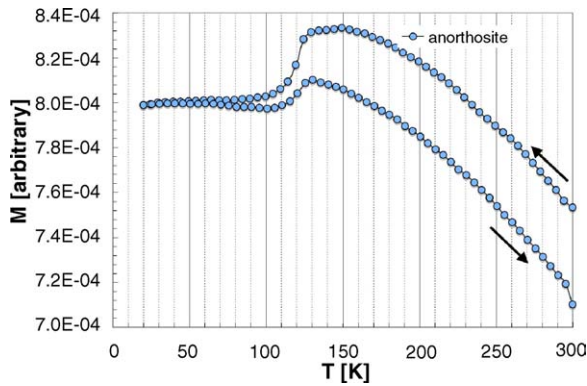
Fig. 2. Following saturation remanence at 300 K, the anorthosite sample containing SD magnetic carriers was temperature cycled in zero field (~1000 nT). Arrows indicate the cooling and heating leg.

For mineralogical verification we measured cryogenic behavior of room temperature saturation remanence by using magnetic properties measurement system – a cryogenic susceptometer by Quantum Design at IRM (Institute for Rock Magnetism), University of Minnesota. We obtained a clear indication of Verwey transition (Fig. 2), another compelling evidence that the tiny SD needles

(Xu et al., 1997) with large aspect ratio (1/50) are indeed SD magnetite crystals.

The iron sample (Iron (IA) coarse octahedrite from meteorite Campo del Cielo) was characterized by scanning electron microscope (SEM) microprobe measurements (only Fe present) and saturation magnetization ($M_s = 190\,\mathrm{Am^2/kg}$). During the thermal acquisition there was no significant decrease of magnetization ($191\,\mathrm{Am^2/kg}$) as shown in Fig. 3D. where hysteresis loop maintain the saturation magnetization of pure iron.

The iron–nickel sample was a polycrystalline industrial product with about 50% nickel, based on SEM microprobe measurements. The value of saturation magnetization was obtained from hysteresis loops ($139\,\mathrm{Am^2/kg}$) and maintained its approximate value also after finishing of the TRM acquisitions ($144\,\mathrm{Am^2/kg}$) as shown by hysteresis loops in Fig. 3C.

The magnetite sample 90LP12 is a non-titanium magnetite obtained from Prof. John Valley, University of Wisconsin. The composition was characterized by x-ray (X-ray diffraction), Curie temperature (565 °C), Verwey transition (120 K), and saturation magnetization ($64\,\mathrm{Am^2/kg}$). Saturation magnetizations (hysteresis
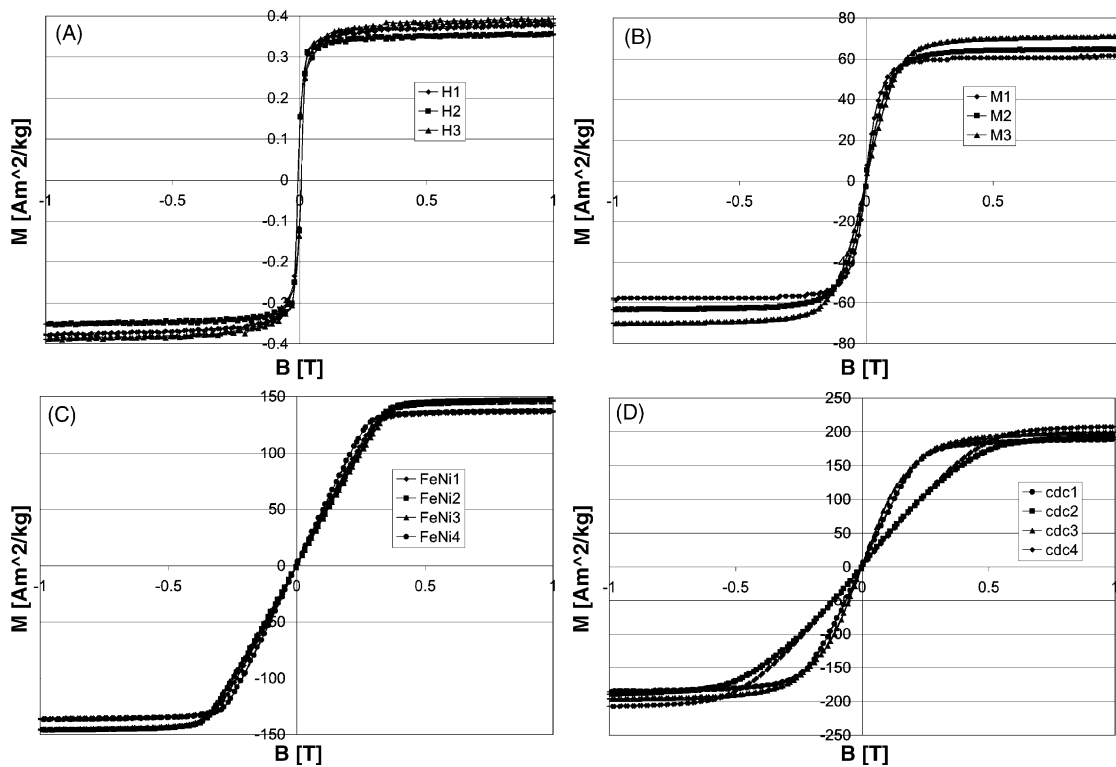

Fig. 3. Hysteresis loops for monomineralic samples after completion of TRM acquisitions. (A) Three hematite samples H1, H2, and H3. (B) Three magnetite samples M1, M2, and M3. (C) Four FeNi polycrystalline grains FeNi1, FeNi2, FeNi3, and FeNi4. (D) Four pure iron samples as part of Campo De Cielo meteorite cdc1, cdc2, cdc3,and cdc4.

loops) were measured both before and after finishing all of the TRM acquisitions (see Fig. 3B.) and registered no change in saturation magnetization (65 Am^2/kg).

The MD hematite sample L2 is a coarse grained variety from the Fire Lake mine in Central Labrador, Canada. Its composition was characterized by x-ray, Curie temperature, Morin transition and saturation magnetization ($M_s = 0.424\ Am^2/kg$). The c-axis of the hematite samples was identified using a vibrating sample magnetometer (VSM). TRM acquisition of hematite samples took place along the basal plane of the mineral ($\pm 5°$). The orientation was maintained based on photographs of the shape of the grains inside the holder for TRM acquisition. For each single crystal sample, the TRM was acquired always along the same direction. Hysteresis loops after all of the TRM acquisitions (Fig. 3A.) indicated slight decrease in M_s ($M_s = 0.38\ Am^2/kg$) but no significant change in mineralogy due to thermal treatment.

For TRM acquisitions each sample was brought to 800 °C in a Shoenstedt oven (except SD M, anorthosite sample that was brought only to 600 °C in a home made oven (SIO)) and held for 30 min in a residual magnetic field fluctuating around 15 nT and ambient atmosphere. Samples were subsequently cooled to room temperature (T_r) while varying the ambient magnetic fields ($\pm 30\%$ of 15 nT; (note that this is the maximum shielding possible and this value is our baseline for complete thermal demagnetization level), $\pm 15\%$ of 80 nT, $\pm 10\%$ of 160 nT, and $< \pm 5\%$ of nominal value for larger fields).

The magnetic field was measured with a Hall probe LakeShore Inc. magnetometer. The field applied in the oven was measured before and after each experiment to insure minimal drifting of the current from the power supply especially for very low fields (e.g., 15 nT).

The magnitude of TRM and SIRM was measured with a superconducting rock magnetometer (SCT – Super-Conducting Technology) (except SD M, which was measured with a 2G magnetometer – SIO) at room temperature and ambient atmosphere. Subsequent magnetic hysteresis loop measurement of each sample provided estimates of saturation magnetization, M_s, and saturation isothermal remanent magnetization, SIRM. The M_s values measured before and after the TRM acquisitions provided a magnetic proxy for unwanted chemical changes that may have occurred during the heating (Fig. 3). However, owing to the large grain size of our samples (~ 1 mm), we did not detect any chemical changes during the thermal treatments. There was no alteration of the SD M sample due to protection of the plagioclase host.

3. Results and discussion

In this work, we focused on determining the lowest field MD single crystals and polycrystalline material could record reliably. The data obtained from the SD magnetite with large aspect ratio is a sample that shows TRM acquisition of SD magnetic carriers. TRM acquisi-

Table 1

Hematite samples were given TRM in paleomagnetic oven where axial field was applied while samples were cooling ($I \sim 0°$, $D \sim 90°$)

H1 M_s: 0.414 A m^2/kg					H2 M_s: 0.413 A m^2/kg					H3 Ms: 0.445 A m^2/kg				
E.F. (nT)	M (Am^2/kg)	I (°)	D (°)	M/SIRM	M (Am^2/kg)	I (°)	D (°)	M/SIRM	M (Am^2/kg)	I (°)	D (°)	M/SIRM
1.5E+01	3.90E−03	−6.3	256.0	9.98E−03	6.9E−03	−4.2	295.3	1.76E−02	7.5E−03	1.4	118.8	1.77E−02
8.0E+01	3.42E−02	−3.1	273.7	8.75E−02	4.8E−03	−3.1	270.6	1.24E−02	2.4E−02	1.9	122.3	5.70E−02
1.6E+02	3.84E−02	7.4	102.9	9.82E−02	1.9E−02	−0.5	183.3	4.94E−02	4.3E−03	1.3	52.0	1.03E−02
3.2E+02	9.89E−03	−6.4	331.3	2.53E−02	7.0E−03	−4.1	338.8	1.79E−02	1.5E−02	0.8	144.2	3.47E−02
6.7E+02	7.44E−03	2.8	96.2	1.90E−02	2.3E−03	3.8	260.5	5.76E−03	8.7E−03	0.6	121.1	2.06E−02
1.4E+03	3.56E−02	1.9	100.3	9.10E−02	1.1E−02	−2.2	3.1	2.76E−02	9.2E−03	−0.4	160.2	2.17E−02
2.8E+03	5.12E−02	3.7	107.8	1.31E−01	2.4E−02	3.7	79.8	6.01E−02	1.3E−02	2.7	94.3	3.07E−02
6.0E+03	4.41E−02	2.7	95.3	1.13E−01	5.0E−02	3.0	111.7	1.27E−01	5.5E−02	2.5	91.8	1.30E−01
1.2E+04	1.56E−01	3.8	72.8	3.99E−01	9.8E−02	4.0	105.4	2.52E−01	1.4E−01	1.7	96.1	3.38E−01
2.4E+04	2.07E−01	3.0	79.8	5.29E−01	1.7E−01	5.8	112.5	4.24E−01	2.3E−01	1.8	89.8	5.35E−01
4.8E+04	2.71E−01	2.3	91.7	6.93E−01	2.2E−01	4.0	105.4	5.64E−01	2.9E−01	2.0	106.3	6.82E−01
9.8E+04	3.20E−01	2.6	91.1	8.19E−01	3.0E−01	4.5	98.1	7.76E−01	3.4E−01	1.8	107.0	8.13E−01
2.0E+05	3.45E−01	4.7	89.2	8.81E−01	3.2E−01	11.0	92.6	8.14E−01	3.7E−01	3.1	100.2	8.71E−01
4.0E+05	3.78E−01	8.6	87.0	9.67E−01	3.2E−01	6.0	120.0	8.31E−01	3.9E−01	3.4	105.5	9.22E−01
8.0E+05	2.79E−01	2.1	130.4	7.14E−01	3.6E−01	4.6	83.7	9.28E−01	3.8E−01	0.2	116.5	9.07E−01
1.6E+06	3.80E−01	−4.6	77.2	9.72E−01	3.6E−01	10.4	114.3	9.08E−01	4.1E−01	2.7	108.7	9.72E−01
SIRM	3.91E−01	2.0	100.4	1.00E+00	3.9E−01	0.8	89.0	1.00E+00	4.2E−01	1.8	89.1	1.00E+00

M_s is the saturation magnetization, E.F. the applied external field, M the TRM acquired by E.F., I the inclination, D the declination, SIRM is the saturation remanence at room temperature.

Table 2

Magnetite samples were given TRM in paleomagnetic oven where axial field was applied while samples were cooling ($I \sim 0°$, $D \sim 90°$)

| E.F. (nT) | M1 M_s: 63.7 A m²/kg | | | | M2 M_s: 67.6 A m²/kg | | | | M3 Ms:74.2 A m²/kg | | | |
	M (Am²/kg)	I (°)	D (°)	M/SIRM	M (Am²/kg)	I (°)	D (°)	M/SIRM	M (Am²/kg)	I (°)	D (°)	M/SIRM
1.5E+01	3.85E−03	−5.1	201.2	1.88E−03	3.35E−03	−19.2	49.3	2.14E−03	3.36E−03	−63.7	203.7	4.22E−03
8.0E+01	7.31E−03	−7.0	129.4	3.57E−03	3.78E−03	−38.8	242.2	2.41E−03	2.36E−03	−34.1	128.9	2.96E−03
1.6E+02	8.03E−03	−13.5	226.6	3.92E−03	4.34E−03	−30.1	214.0	2.76E−03	3.29E−03	−51.4	187.5	4.13E−03
3.2E+02	4.03E−03	1.6	221.8	1.97E−03	3.03E−03	−3.4	267.4	1.93E−03	5.56E−03	−36.9	233.9	6.98E−03
6.7E+02	4.37E−03	−7.6	147.5	2.14E−03	3.69E−03	−3.5	208.0	2.35E−03	4.09E−03	−47.8	78.5	5.14E−03
1.4E+03	6.58E−03	8.4	253.6	3.21E−03	3.15E−03	23.4	161.6	2.00E−03	5.13E−03	−73.1	241.5	6.44E−03
2.8E+03	8.30E−03	−9.2	130.3	4.06E−03	1.79E−03	−39.4	118.1	1.14E−03	4.59E−03	−47.6	186.2	5.76E−03
6.0E+03	4.12E−03	21.6	219.6	2.01E−03	4.83E−03	3.9	94.1	3.07E−03	2.56E−03	−21.0	264.5	3.21E−03
1.2E+04	2.07E−02	6.4	72.6	1.01E−02	6.17E−03	−11.8	93.8	3.92E−03	7.24E−03	0.3	288.8	9.08E−03
2.4E+04	3.23E−02	13.2	116.0	1.58E−02	1.52E−02	2.6	86.4	9.69E−03	5.12E−03	−76.6	283.9	6.43E−03
4.8E+04	2.63E−02	8.1	42.6	1.29E−02	3.26E−02	10.5	83.1	2.08E−02	1.25E−02	1.5	81.0	1.56E−02
9.8E+04	8.16E−02	7.5	81.2	3.99E−02	6.59E−02	3.9	282.7	4.19E−02	2.67E−02	−13.1	94.9	3.36E−02
2.0E+05	2.09E−01	8.3	100.5	1.02E−01	1.39E−01	−1.3	103.1	8.85E−02	4.35E−02	−11.6	78.9	5.46E−02
4.0E+05	2.27E−01	8.9	81.0	1.11E−01	2.37E−01	7.4	109.0	1.51E−01	1.03E−01	−11.6	73.8	1.29E−01
8.0E+05	6.18E−01	7.3	92.1	3.02E−01	4.69E−01	−1.7	102.8	2.99E−01	1.83E−01	−13.8	74.9	2.29E−01
1.6E+06	1.24E+00	0.9	87.6	6.07E−01	7.41E−01	−1.3	108.0	4.72E−01	3.07E−01	−16.8	61.1	3.86E−01
SIRM	2.05E+00	6.0	101.2	1.00E+00	1.57E+00	−2.5	104.1	1.00E+00	7.97E−01	−16.7	79.2	1.00E+00

M_s is the saturation magnetization, E.F. the applied external field, M the TRM acquired by E.F., I the inclination, D the declination, SIRM is the saturation remanence at room temperature.

tion curves (Fig. 1) were determined for acquisition fields ranging from 15 to 10,000,000 nT. All TRM values were normalized by the SIRM acquired at room temperature in an external field of 2 T. For all multidomain material we found an ambient threshold field (TF ~ 1000 nT) below which 1 mm-sized single crystals do not record any variation of ambient field in the resulting TRM (see

Fig. 1 A–D). A similar threshold in TRM acquisition in low fields was found in lunar samples (Dunn and Fuller, 1972). In our samples, TRMs fluctuate in their magnitude and in some extent in direction (Tables 1–4). This is illustrated in Fig. 4, where hematite data from Table 1 of TRM acquisition are plotted on equal area stereographic projections. The diagrams show how the

Table 3

Fe–Ni samples were given TRM in paleomagnetic oven where axial field was applied while samples were cooling ($I \sim 0°$, $D \sim 90°$)

| E.F. (nT) | F2 M_s: 141 A m²/kg | | | | F3 M_s: 145 A m²/kg | | | | F4 M_s: 130 A m²/kg | | | |
	M (Am²/kg)	I (°)	D (°)	M/SIRM	M (Am²/kg)	I (°)	D (°)	M/SIRM	M (Am²/kg)	I (°)	D (°)	M/SIRM
1.5E+01	2.44E−04	−9.8	197.2	4.00E−04	2.74E−04	−31.8	150.9	4.46E−04	1.27E−04	−46.6	133.2	8.15E−04
8.0E+01	3.34E−04	−40.1	232.5	5.48E−04	2.59E−04	−38.9	128.4	4.22E−04	2.12E−04	−47.1	150.8	1.36E−03
1.6E+02	2.20E−04	−67.6	231.4	3.60E−04	2.04E−04	−60.4	177.8	3.32E−04	1.33E−04	−60.7	215.3	8.51E−04
3.2E+02	1.92E−04	−37.3	248.2	3.15E−04	5.43E−05	−37.8	338.0	8.82E−05	8.18E−05	−76.6	198.4	5.24E−04
6.7E+02	2.80E−04	−35.9	237.0	4.59E−04	1.84E−04	−54.2	312.0	2.99E−04	1.10E−04	−31.8	180.5	7.04E−04
1.4E+03	1.72E−04	−34.9	163.7	2.82E−04	2.60E−04	−8.4	76.0	4.22E−04	1.25E−04	−31.1	185.1	8.03E−04
2.8E+03	6.61E−04	−14.6	32.7	1.08E−03	5.22E−04	−3.1	72.2	8.49E−04	1.64E−04	−9.8	124.0	1.05E−03
6.0E+03	8.68E−04	−1.9	95.5	1.42E−03	8.01E−04	−2.8	52.5	1.30E−03	4.23E−04	−8.3	177.1	2.71E−03
1.2E+04	2.12E−03	−7.3	315.4	3.47E−03	1.90E−03	−3.3	68.3	3.09E−03	8.39E−04	−2.0	55.1	5.37E−03
2.4E+04	4.21E−03	7.1	70.5	6.89E−03	4.17E−03	1.7	58.2	6.78E−03	1.74E−03	−1.7	100.5	1.12E−02
4.8E+04	8.97E−03	2.0	73.5	1.47E−02	8.65E−03	−2.5	207.2	1.41E−02	3.41E−03	1.4	98.2	2.18E−02
9.8E+04	1.57E−02	2.8	47.8	2.57E−02	1.71E−02	4.5	94.5	2.78E−02	5.92E−03	1.8	74.6	3.79E−02
2.0E+05	3.12E−02	7.0	93.0	5.12E−02	3.13E−02	10.2	57.2	5.09E−02	9.09E−03	2.8	55.6	5.82E−02
4.0E+05	5.47E−02	4.8	69.0	8.96E−02	5.96E−02	0.2	54.2	9.68E−02	1.66E−02	−2.7	7.8	1.07E−01
8.0E+05	1.06E−01	1.8	141.1	1.73E−01	1.09E−01	8.4	84.5	1.76E−01	2.56E−02	8.0	107.2	1.64E−01
1.6E+06	1.73E−01	2.2	74.6	2.84E−01	1.83E−01	4.0	56.4	2.97E−01	3.77E−02	7.7	71.0	2.41E−01
SIRM	6.11E−01	2.6	99.7	1.00E+00	6.15E−01	2.9	106.7	1.00E+00	1.56E−01	0.5	88.9	1.00E+00

M_s is the saturation magnetization, E.F. the applied external field, M the TRM acquired by E.F., I the inclination, D the declination, SIRM is the saturation remanence at room temperature.

Table 4
Iron samples were given TRM in paleomagnetic oven where axial field was applied while samples were cooling ($I \sim 0°$, $D \sim 90°$)

	Fe1 M_s: 208 Am^2/kg				Fe2 M_s: 202 A m^2/kg				Fe3 M_s: 205 A m^2/kg			
E.F. (nT)	M (Am^2/kg)	I (°)	D (°)	M/SIRM	M (Am^2/kg)	I (°)	D (°)	M/SIRM	M (Am^2/kg)	I (°)	D (°)	M/SIRM
4.0E+01	1.68E−04	−14.6	252.7	9.59E−05	5.80E−04	−20.2	330.1	3.37E−04	2.83E−04	−35.1	213.2	1.54E−04
8.0E+01	3.10E−04	−37.4	186.0	1.77E−04	2.98E−04	−8.2	82.8	1.73E−04	5.54E−04	−22.5	140.3	3.00E−04
1.6E+02	3.70E−04	−13.4	105.0	2.11E−04	1.10E−03	−15.0	260.3	6.37E−04	4.37E−04	−21.6	239.7	2.37E−04
3.5E+02	3.05E−04	26.3	51.7	1.74E−04	3.10E−04	−69.8	5.9	1.80E−04	3.07E−04	−30.2	257.7	1.66E−04
5.5E+02	8.70E−04	−58.2	49.9	4.96E−04	5.68E−04	−69.2	14.6	3.30E−04	5.21E−04	−29.7	287.4	2.83E−04
1.4E+03	8.70E−04	−4.6	25.7	4.96E−04	6.14E−04	10.3	24.4	3.57E−04	4.17E−04	31.9	13.1	2.26E−04
2.8E+03	3.45E−04	18.6	113.6	1.97E−04	9.46E−04	7.5	236.8	5.49E−04	5.77E−04	−4.8	252.7	3.13E−04
6.0E+03	1.43E−03	−11.6	80.9	8.13E−04	3.04E−03	1.6	65.7	1.76E−03	2.17E−03	−15.1	332.2	1.18E−03
1.2E+04	1.77E−03	−11.5	81.1	1.01E−03	3.94E−03	5.5	71.9	2.29E−03	2.53E−03	4.9	151.3	1.37E−03
2.4E+04	3.92E−03	−7.5	257.8	2.24E−03	6.40E−03	9.1	299.4	3.72E−03	4.61E−03	−8.1	323.0	2.50E−03
4.8E+04	9.23E−03	7.6	86.8	5.27E−03	1.36E−02	3.5	126.3	7.88E−03	1.61E−02	0.5	111.5	8.74E−03
9.8E+04	1.56E−02	−17.1	6.0	8.91E−03	1.99E−02	4.6	141.3	1.16E−02	2.94E−02	−0.1	111.7	1.60E−02
2.0E+05	4.55E−02	19.5	59.6	2.59E−02	7.16E−02	−8.4	99.1	4.16E−02	7.14E−02	3.0	91.1	3.87E−02
4.0E+05	1.15E−01	1.4	252.4	6.57E−02	1.44E−01	6.8	80.7	8.39E−02	1.58E−01	1.4	81.2	8.56E−02
8.0E+05	1.81E−01	−2.1	42.8	1.03E−01	2.77E−01	−6.0	105.4	1.61E−01	2.81E−01	4.1	82.2	1.53E−01
1.5E+06	3.78E−01	3.7	130.1	2.16E−01	3.59E−01	−20.4	212.2	2.08E−01	5.71E−01	0.1	78.5	3.10E−01
SIRM	1.75E+00			1.00E+00	1.72E+00			1.00E+00	1.85E+00			1.00E+00

M_s is the saturation magnetization, E.F. the applied external field, M the TRM acquired by E.F., I the inclination, D the declination, SIRM is the saturation remanence at room temperature.
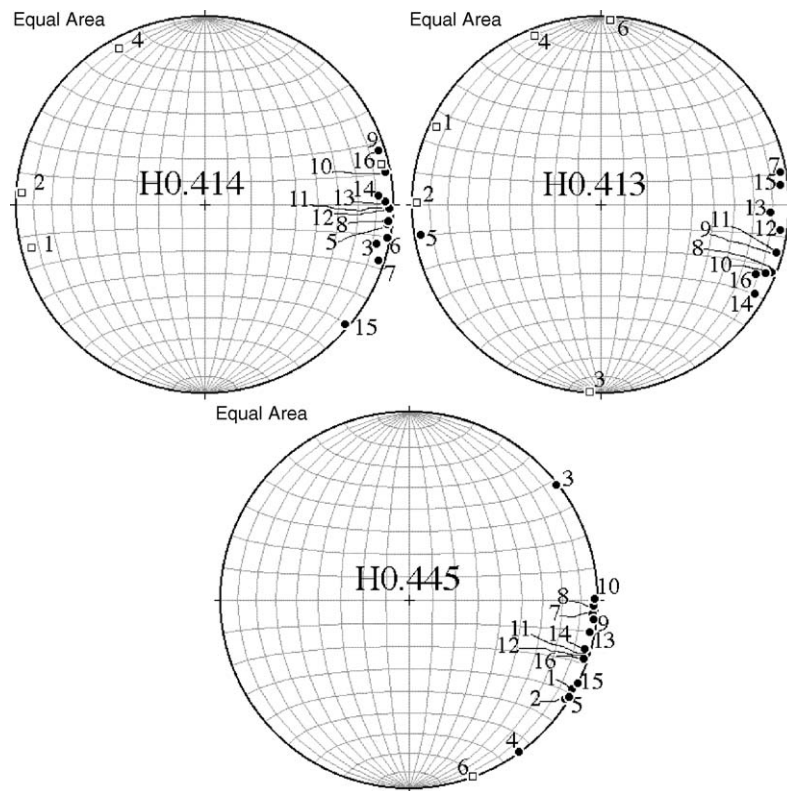

Fig. 4. Directional behavior of hematite samples during the TRM acquisition is shown with stereonet equal area projection. Samples are identified by their saturation magnetization value (in Am^2/kg) shown in Figs. 1 and 2. The c-axis of the samples was perpendicular to the acquisition field (90° plunge in the stereonet projection). The field was applied from left to right. The small numbers next to data points denote the acquisition fields (1 = 15, 2 = 80 nT, and so on, see Table 1).

vector of magnetization stays within the basal plane of hematite. Since our samples are not perfect spheres but have irregular shape the magnetic direction is controlled by the shape anisotropy due to the demagnetizing field. In hematite, the magnetization is confined to the basal plane due to the strong magnetocrystalline anisotropy and the shape anisotropy is relevant only within this basal plane. Samples recorded similar magnetic directions below the observed threshold field value, however with TRM intensity fluctuating around a constant value. For fields < 1000 nT TRM of any MD grains (∼1 mm in diameter) are not affected by changes in the applied external magnetic fields. This brings about a domain state independent of the inducing field because of the total dominance of the demagnetizing energy. Finite TRM level for low acquisition magnetic fields is particularly important for studies with lunar rocks and meteorites, where the ambient magnetizing fields may have been in 1000 nT range or lower and where there is a large abundance of coarse-grained magnetic minerals.

We have considered the possibility that values of TRM could be contaminated by a VRM or IRM imparted by the laboratory ambient field. After samples were cooled in the controlled field down to room temperature they were transported to the superconducting rock magnetometer while being exposed to the ambient field of the laboratory. In order to resolve this problem the first author visited two shielded rooms, one in Heidelberg University in Germany run by Agnes Kontny, and another one in Scripps Institution of Oceanography in USA run by Lisa Tauxe and duplicated experiments with MD hematite grains. Both of these labs had the background field reduced by at least two orders of magnitude. Hematite samples were shielded down to <800 nT during the transport and still produced similar values of TRM as in the Goddard lab where the room temperature transport of the sample to the magnetometer was not shielded.

The threshold field for hematite (Fig. 1A) leaves large portion of the thermoremanent magnetization (1–10% of SIRM) after thermal cycling in the lowest magnetic field. Neel theory (straight line in Fig. 1A.) does not account for the finite number of domains and therefore fail to predict this demagnetizing threshold. High level of remanence left in the monomineralic sample decreases with an increase of the material's saturation magnetization (e.g. <0.1% for iron sample, see Fig. 1D). The observed TRM/SIRM sensitivity (Fig. 1) at the threshold field (TF) of ∼1000 nT for all of the minerals should relate with the number of domains in the magnetic grain. If, for example, we have a hypothetical single domain grain 1 mm in

size, the TRM/SIRM should have a maximum value and there should be no TRM acquisition variation due to the single domain nature of this grain.

Fig. 1A shows that single crystals (1 mm) of hematite attain the highest value of TRM/SIRM below the TF. Hematite has relatively large domains compared with all other magnetic carriers and thus there are only a small number of domains within the 1 mm single crystal of hematite. The data in Fig. 1A suggest that domains can rearrange to achieve the minimum magnetization of 2–8% of SIRM.

Magnetite grains (Fig. 1 B) contain smaller domains size and demagnetize down to 0.2–0.6% of SIRM. Iron–nickel and iron grains (Fig. 1C and D) have even smaller domain size and hence more domains, and our data suggest that these magnetic grains can be demagnetized down to 0.03–0.09% and 0.02–0.06% of their SIRM, respectively.

Fig. 1B includes the data of SD magnetite sample SD M, (anorthosite host), composed of single domain magnetite needles (see material and method section and Fig. 2). TRM acquisition of this sample is not affected by threshold seen for multidomain magnetite. Large number of SD grains within the plagioclase matrix effectively randomizes their moment and allow effective TRM threshold to drop down to less than 100 nT. The overall enhanced efficiency of TRM reflects the high aspect ratio up to 1:50 (Xu et al., 1997) and relates to a decrease of demagnetizing field during TRM acquisition (Kletetschka et al., 2004).

Fig. 5 summarizes all MD mineral data into one diagram for clarity. This plot shows clearly how both the level of demagnetization as well as efficiency of TRM acquisition relate to saturation magnetization. This fur-
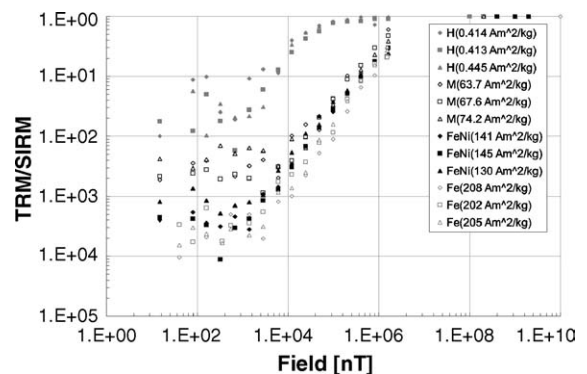

Fig. 5. Summary plot of SIRM normalized TRM for monomineralic magnetic grains (H = hematite, M = magnetite, FeNi = iron–nickel, Fe = iron) vs. inducing artificial homogeneous external magnetic field. Note that numbers shown in the legend are saturation magnetizations of individual samples.

ther constrain recently discovered general empirical relationship (Kletetschka et al., 2004).

The results described in this contribution have implications for paleointensity determinations of samples where multidomain grains are abundant. However, we stress that these results are obtained on mono-mineralic samples. In reality, samples are assemblages of multiple magnetic grains of various shapes and composition. However, a rock may contain only one magnetic carrier (e.g., magnetite) and represented by a distribution of magnetic grains. An increase in the quantity of the magnetic grains or carriers would further randomize the TRM and the threshold field should drop below the threshold observed in our measurements of individual mineral grains (e.g., SD M in Fig. 1B).

4. Conclusions

The TRM efficiency data acquired in very low fields for single grains of hematite, magnetite, iron–nickel, and iron revealed the existence of finite plateau (magnetization level) starting at $1\,\mu T$ below which the acquired TRM is unreliable. The large MD-grain TRM in fields below $1\,\mu T$ becomes independent of the field and this "noise level" of TRM decreases with increasing spontaneous magnetization. We interpret this threshold as a consequence of the number of domains within the volume of magnetic mineral. The knowledge of these threshold levels is critical for paleofield estimates made from extraterrestrial material because they can experience much weaker TRM acquisition fields than terrestrial rocks and they often contain large MD grains of magnetic minerals.

Acknowledgements

References

Bergh, H., 1970. Paleomagnetism of the stillwater complex. In: Runcorn, S. (Ed.), Paleogeophysics. Academic Press, London, pp. 143–158, Chapter 17).

Brown, W.F., 1959. Relaxational behaviour of fine magnetic particles. J. Appl. Phys. 30, 130S–132S.

Butler, R.F., Banerjee, S.K., 1975. Theoretical single-domain grain size range in magnetite and titanomagnetite. J. Geophys. Res. 80, 4049–4058.

Day, R., 1977. TRM and its variation with grain size: a review. J. Geomagn. Geoelectr. 29, 233–265.

Dunlop, D.J., Kletetschka, G., 2001. Multidomain hematite: a source of planetary magnetic anomalies? Geophys. Res. Lett. 28 (17), 3345–3348.

Dunlop, D.J., Waddington, E.D., 1975. The field dependence of thermoremanent magnetization in igneous rocks. Earth Planet. Sci. Lett. 25, 11–25.

Dunlop, D.J., Özdemir, Ö., 1997. Rock Magnetism: Fundamentals and frontiers. Cambridge Studies in Magnetism, vol. 3. Cambridge University Press, Cambridge, 573 pp.

Dunn, J.R., Fuller, M., 1972. Thermoremanent magnetization (TRM) in lunar samples, Lunar Geophysics – The Moon, pp. 197–209.

Everitt, C.W.F., 1962. Thermoremanent magnetization II: experiments on multidomain grains. Phil. Mag. 7, 583–597.

Kletetschka, G., 2000. Intense remanence of hematite–ilmenite solid solution. Geol. Carp. 51 (3), 187.

Kletetschka, G., Acuna, M.H., Kohout, T., Wasilewski, P.J., Connerney, J.E.P., 2004. An empirical scaling law for acquisition of thermoremanent magnetization. Earth Planet. Sci. Lett. 226 (3–4), 521–528.

Kletetschka, G., Wasilewski, P.J., Taylor, P.T., 2002. The role of hematite – ilmenite solid solution in the production of magnetic anomalies in ground and satellite based data. Tectonophysics 347 (1–3), 166–177.

Merrill, R.T., 1977. The demagnetization field of multidomain grains. J. Geomagn. Geoelectr. 29, 285–292.

Néel, L., 1949. Théorie du traînage magnétique des ferromagnétiques en grains fins avec applications aux terres cuites. Ann. Géophys. 5, 99–136.

Néel, L., 1955. Some theoretical aspects of rock magnetism. Adv. Phys. 4, 191–243.

Robinson, P., Harrison, R.J., McEnroe, S.A., Hargraves, R.B., 2002. Lamellar magnetism in the haematite–ilmenite series as an explanation for strong remanent magnetization. Nature 418, 517–520.

Schmidt, V.A., 1973. A multidomain model of thermoremanence. Earth Planet. Sci. Lett. 20, 440–446.

Selkin, P.A., Gee, J.S., Tauxe, L., Meurer, W.P., Newell, A.J., 2000. The effect of remanence anisotropy on paleointensity estimates: a case study from the Archean stillwater complex. Earth Planet. Sci. Lett. 183, 403–416.

Stacey, F.D., 1958. Thermoremanent magnetization (TRM) of multidomain grains in igneous rocks. Phil. Mag. 3, 1391–1401.

Xu, W., Geissman, J., Voo, R.v.d., Peacor, D., 1997. Electron microscopy of iron oxides and implications for the origin of magnetizations and rock magnetic properties of Banded Seriesrocks of the stillwater complex, Montana. J. Geophys. Res. 102, 12139–12157.